NUMERICAL SIMULATION AND DESIGN OF HYBRID OSCILLATING HEAT PIPE-

PHASE CHANGE MATERIALS FOR RADIATOR PANEL


A Thesis

by

AASHIK SHRESTHA



Submitted to the Graduate and Professional School of
Texas A&M University
in partial fulfillment of the requirements for the degree of

MASTER OF SCIENCE



| | |
|---|---|
| Chair of Committee, | Patrick Shamberger |
| Committee Members, | Ankit Srivastava |
| | Choongho Yu |
| Head of Department, | Ibrahim Karaman |


May 2022

Major Subject: Material Science and Engineering

ABSTRACT

Effective thermal management is a challenge in spacecrafts due to demands of higher power operating sensors and devices in satellites resulting in high-temperature rise. The use of a two-phase passive heat transfer device, such as oscillating heat pipes (OHPs), can effectively increase heat transfer rate and spread out heat as a radiator panel due to its lightweight, high performance, and reliability. However, OHPs have limited thermal capacitance and thus, remain susceptible to rapid temperature rise during periods of transient high-power operation. Integrating phase change materials (PCMs) with OHP radiator panels can serve to buffer temperature below a key target temperature for some period of time due to the latent heat of PCMs. Here, we present a validated reduced-order numerical model for a hybrid OHP-PCM slab and apply this model to analyze the transient thermal response of a hybrid OHP-PCM radiator panel. This model is validated against experimental data collected from an OHP panel. We apply this model to assess design tradeoffs associated with panel geometry and material thermophysical properties. The transient thermal loading conditions of the hybrid OHP-PCM panel is observed for different PCMs, including octadecane, gallium, and composite material (with relative volume fractions of 0.9 octadecanes and 0.1 aluminum). The transient temperature rise under loads of 1 kW, 3 kW, and 10 kW were evaluated for different thickness of PCMs, ranging from 0.001 m to 0.01 m. The area of hybrid OHP-PCM radiator panel is 0.25 $m^2$. The hybrid OHP-PCM model for octadecane is limited by the rate of heat transport due to low thermal conductivity. However, gallium and composite (with 0.9 VF octadecane and 0.1 VF aluminum) are not limited by the rate of heat transport due to high thermal conductivity but rather are limited by the volume of the system. Similarly, for a desired thermal buffering time, the composite material takes less mass to reach the same temperature

during the transient state compared to gallium. The numerical model can be used as a design tool to investigate the mass and volume tradeoffs of hybrid OHP-PCM panels.

DEDICATION

This work is dedicated to my mother, father, sister, and friends who have helped me through

every step in life to become a better and more responsible person.

# ACKNOWLEDGEMENTS

I would like to thank my committee chair and advisor. Dr. Shamberger for providing research opportunities and continuous guidance throughout the course of this research. I would also like to thank my committee members, Dr. Srivastava and Dr. Yu, for their guidance and support with my thesis dissertation.

I would like to thank my friends and colleagues for making my time at Texas A&M University a great experience.

I would also like to thank Rikky for her continuous support and motivation throughout my time at Texas A&M University.

# CONTRIBUTORS AND FUNDING SOURCES

## Contributors

This work was supported and supervised by a thesis committee chair Dr. Shamberger and committee member Dr. Srivastava of the Department of Material Science and Engineering and committee member Dr. Yu of the Department of Mechanical Engineering.

## Funding Sources

TABLE OF CONTENTS

# LIST OF FIGURES

# LIST OF TABLES

# 1. INTRODUCTION

Thermal management is a challenge in spacecraft for electronics and radiator panels due to the use of high power and small thermal mass devices, which causes limited heat transport and overheating of electronic components [1-3]. The use of two-phase passive heat transfer devices, such as oscillating heat pipes (OHPs), can provide better heat transport due to high thermal conductivity and low mass [4-7]. However, due to the low thermal capacitance, the performance of OHPs is limited for large operating temperature and transient thermal loading conditions [8]. To improve the performance of OHPs during transient loading conditions, thermal energy storage materials, such as phase change materials (PCMs) that have a high energy density, could be integrated with OHPs, to increase the effective thermal capacitance of the system [9-11]. However, the study of the overall system performance of hybrid OHP-PCM panels for different geometries, the interaction of OHPs with different PCM properties, and under different heat loading conditions is still lacking and requires further investigation. The hybrid OHP-PCM panel design tradeoffs and interaction of different PCMs with OHP at different power inputs are studied using the finite difference method for a reduced order numerical model.

## 1.1 Traditional Heat Pipe

Heat pipes are heat transfer devices with a high thermal conductivity that consists of internal wick structure with working fluid such as water, ammonia that has both vapor and fluid for a desired operating temperature range [12]. The working mechanism of a traditional heat pipe is based on capillary action due to the internal wick structure. Fig. 1 represents the working mechanism of a heat pipe. The heat pipe is divided into three sections; evaporator, adiabatic, and condenser section. The heat source is provided in the evaporator section where working fluid changes to vapor form.

Due to high pressure at the vapor section, the vapor moves to the condenser region where heat sink is present.
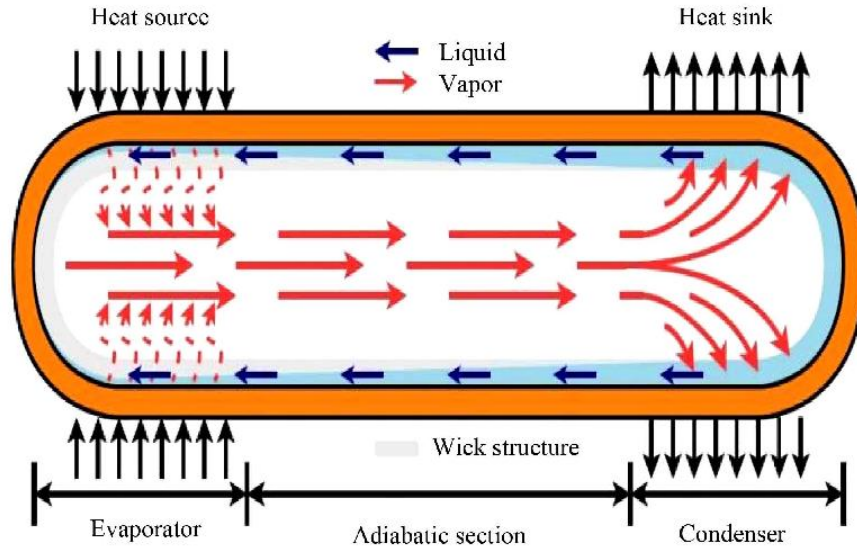


Figure 1: Working mechanism of traditional heat pipe. Reprinted from Creative Commons Attribution License [12]

At the condenser, the vapor again turns into liquid. The liquid then flows back into evaporator section through capillary action due to the wick structure present inside traditional heat pipe. Heat pipes have been used in applications from computer cooling devices to spacecraft thermal control, where inclination angle of heat pipe and physical properties of the working fluid have significant effect for optimized cooling [12, 13]. The maximum thermal conductivity and heat transport capability of traditional heat pipes for rectangular, triangular and circular geometries has been studied for increased power levels. [14-16]. The FEM analysis was performed using ANSYS for all three geometries with Copper as the base material for wick structure and as an envelope because of better thermal and mechanical properties to withstand corrosion [17, 18]. The maximum effective thermal conductivity was reported for square heat pipe with a value of $4018 \ \mathrm{W \cdot m^{-1} \cdot K^{-1}}$ by measuring the temperature difference from source to sink [18, 19].

## 1.2 Oscillating Heat Pipe

The high sensitivity to orientation and cost of manufacturing conventional heat pipes due to internal wick structure has led to the development of a new type of heat transfer device with high dissipating-heat power by Akachi in the 1990s called as oscillating heat pipes (OHPs) [7, 20]. OHPs consist of capillary tube and are divided into three sections called as heating section, the adiabatic section, and the cooling section. Fig. 2 represents a schematic figure of OHPs. The working mechanism of oscillation inside OHPs occurs when the fluid inside heating section boils, expanding the vapor bubbles. The vapor bubbles travel through adiabatic section to the cooling section, where vapor bubbles contract. The expansion and contraction of vapor bubbles create a difference in pressure between heating and cooling section resulting in an oscillation of working fluid. The operation limitation of OHPs to determine maximum heat transport capability has been studied experimentally, where OHPs depend on working fluid filling ratio and heat flux [8]. The experimental study of three-layer OHPs were also performed to determine the effect of channel layers during high power with maximum effective thermal conductivity of $33,170 \text{ W} \cdot \text{m}^{-1} \cdot \text{K}^{-1}$ [21].
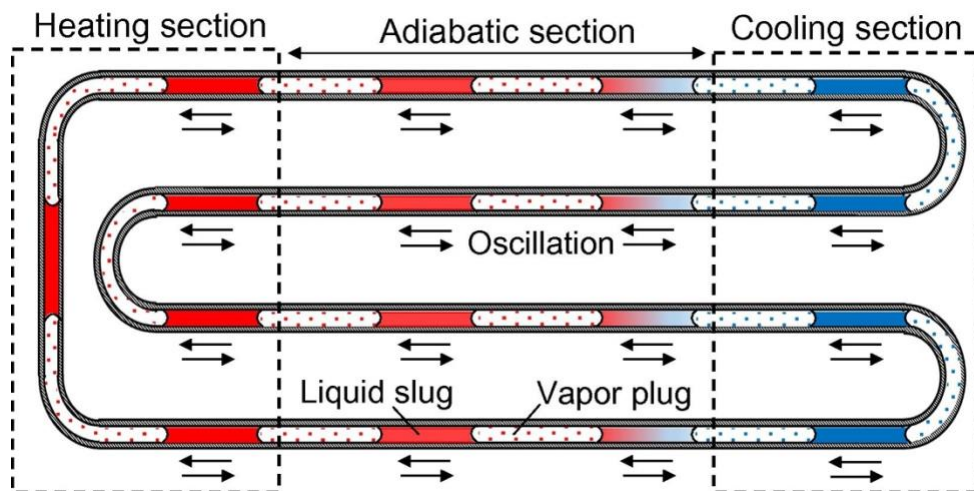


Figure 2: Schematic of Oscillating heat pipe. Reprinted with permission from Elsevier [4]

3

Better performance of closed-loop pulsating heat pipes has been shown in most studies where higher number of turns result in better circulation of working fluid and formation of oscillation wave [22-24]. Experimental study for several working fluids (e.g. water, ethanol) and nanofluids inside OHPs have been done to observe heat transfer mechanism and flow visualization [25-28]. Xian et. al. [25] performed an experiment to understand operating behavior for two different working fluids of water and ethanol with better thermal performance for water. Ma et. al. [29] performed numerical modeling of the oscillating heat pipe to study heat transfer mechanism through forced convection which showed better heat transfer through the oscillation process. An experimental investigation was performed to validate the numerical modeling which showed the oscillation motion occurred when there was an onset temperature difference between evaporator and condenser region resulting in a better heat transfer [29]. The operation limitation of OHPs is dependent on the oscillation motion of liquid slug and vapor plug, the diameter of the pipe, fluid filling ratio, and under different heat flux conditions [30, 31]. An explicit finite difference method was modeled to determine the heat transfer rate with simplified assumptions of OHPs and validated against the experimental work [32]. Shafii [33] presented governing equations using the explicit finite difference method, where gravity has negligible effect and heat transfer occurs mainly due to sensible heat of OHPs. The mathematical model for one dimensional flow of closed loop OHPs for ideal vapor flow, negligible surface tension and drag force due to frictional force between vapor, liquid and the wall was assumed and calculated using numerical solution, where velocity of liquid depends on the temperature difference between evaporator and condenser section [34].
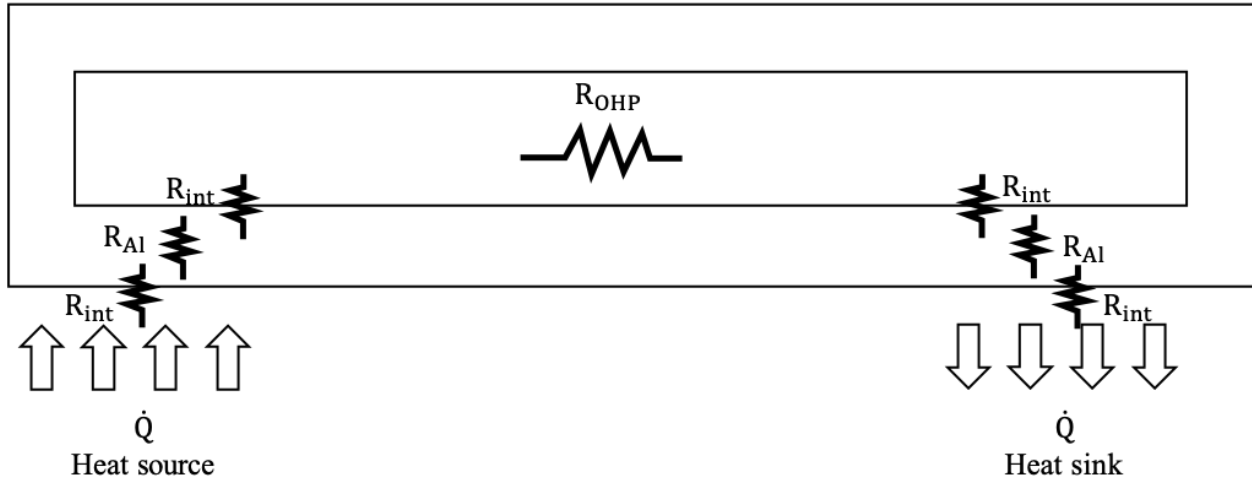
Figure 3: 1D thermal resistance network model for OHP enclosed in Aluminum

Fig. 3 represents the 1D thermal resistance network where resistance of Closed Loop OHPs enclosed in Al material is shown. The overall thermal resistance is a sum of all individual resistance of materials included. The thermal resistance of OHP depends on the working fluids and filling ratio that provide lower thermal resistance of the system [35]. Khandekar et al. [36] reported better thermal performance for a volumetric filling ratio between 15-25% for water and 55% for ethanol. The transient thermal response of OHP was calculated using a reduced-order numerical model through finite different method for cartesian geometry system for high thermal conductivity of OHP with introduction of interfacial resistance that closely matches the results with experimental measurements [37].

1.3 Phase Change Materials

Phase Change Materials (PCMs) are thermal energy storage materials with high latent heat storage properties and plays important role in the thermal management system [38, 39]. Fig. 4 represents the schematic of phase change material temperature-time transition. As the temperature is increased for a PCM, the energy gets stored in sensible heating with an increase in temperature.

However, after reaching the phase change temperature, the temperature remains constant with absorption of energy over time until it completely exhausts latent heat energy.
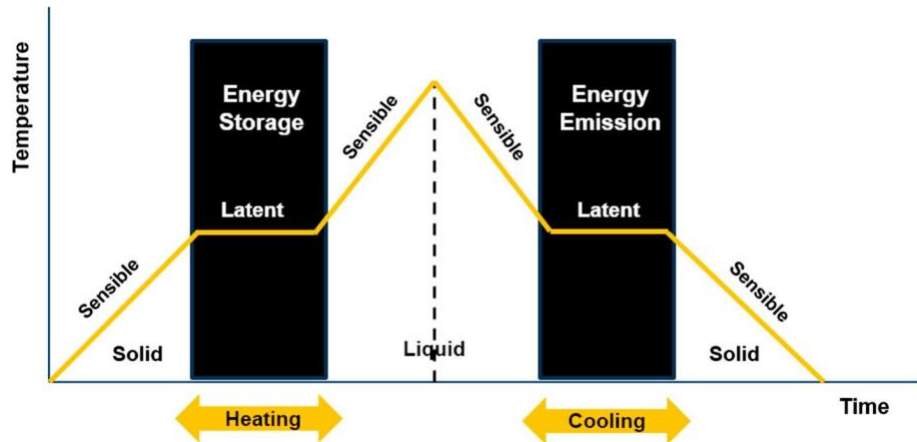


Figure 4: Schematic of phase change material temperature-time transition. Reprinted with permission from Elsevier [39]

Due to the nature to absorb more heat with constant temperature for a certain amount of time PCMs can be used for transient thermal load applications for high power electronics, batteries, solar PV, vehicles, and spacecraft [40-43]. There are different types of PCMs used to manage thermal loads such as salt hydrates, paraffin, metals and composite PCMs. PCMs with high latent heat of fusion, high density, corrosion resistance and high thermal conductivity is desired for space applications as the only source of rejecting heat out of the system is through radiation. Due to the corrosive nature of salt hydrates, they are generally not considered for spacecrafts applications. However, use of paraffin is generally found in spacecraft due to high latent heat of fusion, cost effective and non-reactive with other materials [44, 45]. The numerical simulation was performed for shape stabilized PCM at spacecraft thermal system against the damage of transient high heat flux, with use of multilayer insulation (MLI), shown in Fig. 5, where the use of PCM maintains the operating temperature limit and protects the spacecraft device [44]. As there are different classifications of

PCM materials from organic to inorganic PCM compounds, recent experimental evaluation have been performed for a metallic PCM compound and organic PCM compound for thermal buffering at high power [46]. In the experiment performed by Gonzalez et. al. [46], the metallic PCM compound showed temperature suppression of up to 60% by replacing with an organic PCM compound. In comparison to using dielectric gel, 80 ℃ difference in temperature is achieved for short pulses of metallic PCM compound for same temperature rise.
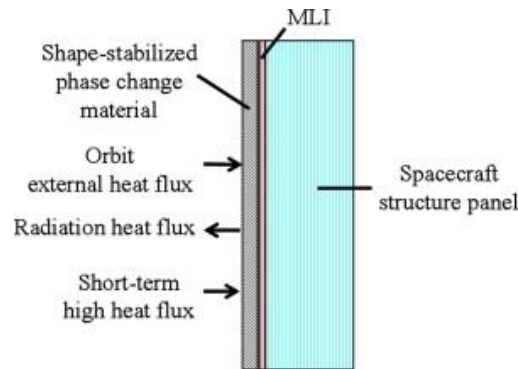
Figure 5: Schematic diagram of use of Phase Change Material in Spacecraft structure. Reprinted with permission from Elsevier [44]

Similarly, for 1D non-linear heat transfer analytical solution, metallic PCM show less temperature rise compared to organic PCM under 20 ms pulse with better performance and thermal conductivity of metal PCM compound [47, 48]. The numerical solution using finite difference method for cooling components using PCM composite has been defined for cartesian and cylindrical geometry system under different boundary conditions [49-51].

1.4 Hybrid OHP-PCM system

The study of traditional heat pipes coupled with PCMs has been conducted for better transient thermal performance of electronics to reduce the temperature rise [52, 53]. Weng et. al [52] performed the study of heat pipe coupled with different PCMs at the adiabatic section. The thermal performance of heat pipe coupled with tricosane resulted in a 46% decrease in power consumption

as compared to the traditional heat pipe. The study of traditional heat pipe enclosed with PCMs in the adiabatic region for a different filling ratio of paraffin wax has been experimentally conducted by Zhuang et. al [54]. The closed heat pipe with a 75% filling rate of paraffin wax had a 9.31% temperature drop compared to the 0% filling rate of the paraffin [54]. The numerical model study of heat pipe-chase change material using thermal resistance network approach for spacecraft radiator panel compared the system with and without the addition of PCMs, where the addition of PCMs decreased overall system temperature [53]. The numerical study also resolved the issue of low thermal conductivity of PCMs by arranging the PCMs in parallel to the heat pipes.

The thermal performance for battery management based on oscillating heat pipe-phase change materials has been studied that shows better cooling performance to decrease the temperature of the battery [55, 56]. The thermal performance of OHP in spacecraft has higher transport capability compared to traditional heat pipe as the difference in the performance of OHP on orbit and on the ground is relatively small [4, 57]. The traditional heat pipe has been known to show performance degradation in a gravitational field due to weak force present during capillary action because of wick structure [20]. However, flat plate oscillating heat pipe shows no performance degradation under gravitational field and can be applied for micro gravitation field. The experimental and numerical study of flat plate oscillating heat pipe with check valve has been carried out in space where no performance degradation has been shown for about 4 years [4, 58]. However, the study of oscillating heat pipe coupled with phase change materials for design geometry optimization and effect of thermophysical properties of PCMs at different power for thermal buffering is still lacking and requires further study.

1.5 Scope of the study of hybrid OHP-PCM system

Here, we present the numerical study of oscillating heat pipe coupled with phase change materials under radiation boundary conditions for effective thermal performance during transient loading conditions by using the finite volume method with simplified assumptions of OHP and PCMs for model geometry optimization. The melting behavior of different types of PCMs with OHP at different ranges of heat flux is studied to assess design tradeoffs and thermophysical properties of the materials. The rate limited and volume limited case of hybrid OHP-PCM panel for different PCMs is analyzed. This numerical model can be used as a design tool to determine mass and volume tradeoffs of hybrid OHP-PCM system.

## 2. METHODS[*]

2.1 Model Geometry / System of Study

Rectangular and cylindrical model geometries are developed for the study of hybrid OHP-PCM panels. The numerical model geometry consists of OHP and PCMs enclosed in the Aluminum (Al) layer as shown in Fig. 6c. Fig. 6a represents the rectangular model geometry and Fig. 6b represents cylindrical model geometry. The rectangular model heat transport occurs in only one direction along with the height of the OHP channel. Due to the limitation of heat transfer to occur only across the panel linearly, the cylindrical model is developed for even heat transfer in all directions.
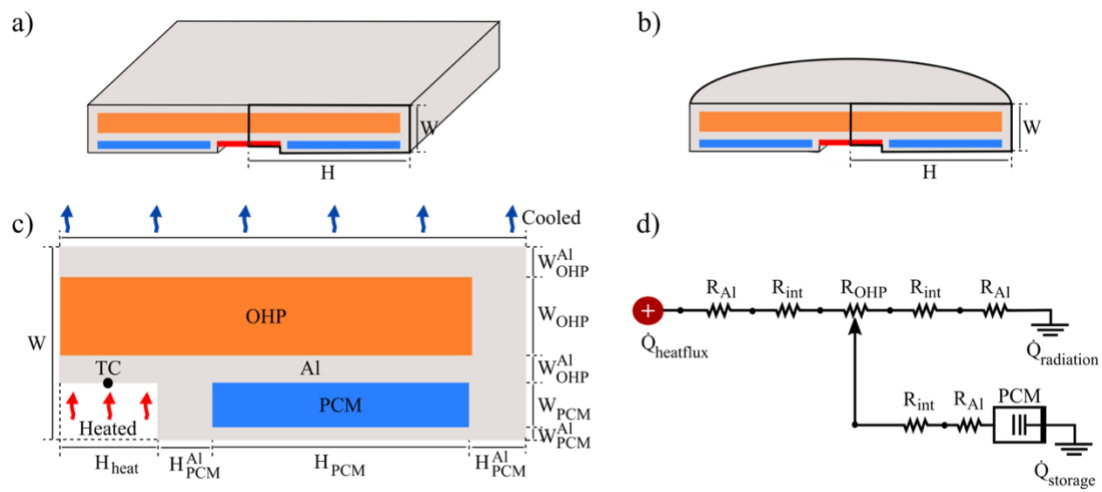


Figure 6: a) Rectangular model b) cylindrical model c) Cross section view for both rectangular and cylindrical model geometry of hybrid OHP-PCM slab d) 1D resistance model

The OHP slab is treated homogeneously with a volume fraction of properties of Al and fluid-filled channels (E.g. ethanol). Fig. 6c represents the cross-section panel view of both rectangular and cylindrical models where heat is flowing from top to bottom of the panel. The boundary condition selected for this model is constant heat flux on hot side and radiation boundary condition on cooling side for top surface. The remaining boundaries are considered adiabatic.

For the case study of a cylindrical and rectangular model of hybrid OHP-PCM panel, three materials performance is measured for PCMs; octadecane, gallium, and composite (with 0.9 VF octadecane and o.1 VF Al). The filling ratio of working fluid (ethanol) used is 50% for the maximum heat transport [59]. The materials properties of all three PCMs are provided in Table 1. The thermal conductivity of OHPs parallel to fluid flow is 320000 $W \cdot m^{-1} \cdot K^{-1}$ and along the width and depth is considered 20 $W \cdot m^{-1} \cdot K^{-1}$ for the validation. However the thermal conductivity value is considered isotropic for other materials present in the model. The thermal resistance network consisting of both OHP and PCM material for given model geometry is represented in Fig. 6d. The 1D resistance model represented in Fig. 6d shows the direction of heat flow from a heat source to a heat sink with all thermal resistance in between the materials. $R_{Al}$ is the resistance of aluminum, $R_{OHP}$ is the resistance of oscillating heat pipe and $R_{int}$ is the interfacial resistance between two materials.

Table 1: List of Materials with their properties considered in this study. Reprinted with permission from AIP and Elsevier [60-64]

| Materials | $\rho$ $\left(\dfrac{kg}{m^3}\right)$ | $C_{p\_l}$ $\left(\dfrac{J}{kg.K}\right)$ | $C_{p\_s}$ $\left(\dfrac{J}{kg.K}\right)$ | $\Delta H$ $\left(\dfrac{J}{kg}\right)$ | $T_m$ (°C) | $k_x$ $\left(\dfrac{W}{m.K}\right)$ | $k_x$ $\left(\dfrac{W}{m.K}\right)$ | $k_z$ $\left(\dfrac{W}{m.K}\right)$ |
|---|---|---|---|---|---|---|---|---|
| Al 6063 | 2700 | 900 | 900 | 1 | 616 | 200 | 200 | 200 |
| OHP (Ethanol) | 790 | 2460 | 0 | 0 | 0 | 20 | 320000 | 20 |

| | | | | | | | | |
|---|---|---|---|---|---|---|---|---|
| Octadecane (paraffin) | 774 | 2160 | 1800 | 244186 | 28 | 0.358 | 0.358 | 0.358 |
| Gallium | 6093 | 400 | 340 | 80091 | 29.8 | 33.5 | 33.5 | 33.5 |
| PCM Composite | 966 | 1808 | 1548 | 175977 | 28 | 20.3 | 20.3 | 20.3 |

The value of interfacial resistance present between two materials is $2.0 \times 10^{-6} \, \text{m}^2 \cdot \text{K} \cdot \text{W}^{-1}$ [37]. $\dot{Q}_{\text{heatflux}}$ is constant heat flux boundary condition and $\dot{Q}_{\text{radiation}}$ is radiation boundary condition at cooling surface. $\dot{Q}_{\text{storage PCM}}$ is the latent heat storage of PCM where excess heat is stored until the PCM reaches melting temperature. The resistance network is connected in series with PCM connected in parallel to the rest of the model. Due to the latent heat storage property of PCM, it can absorb excess heat or also serve as a radiator panel until the melting point of PCM if no other cooling condition is present.
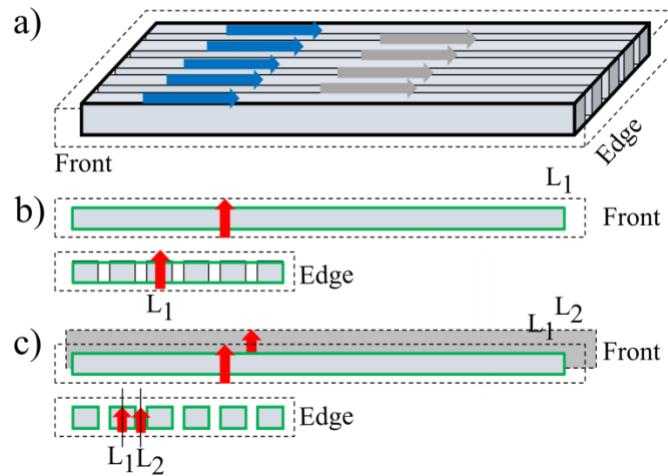


Figure 7:a) Model geometry set-up. b) cross-section view for 2D model (front and edge) b) cross-section view of 2D 2Layer model (front and edge)

The model geometry consisting of parallel OHPs with the direction of heat flow is presented in Fig. 7a. Fig. 7b represents the 2D model of the slab where interfacial resistance is present only in between the layers of Metal (Al) and OHP structure. In this model, the OHP slab (which consists of both Al support structures and fluid-filled channels) is treated as a homogeneous slab (with

properties proportional to the volume fractions of the two constituent elements). The path of heat transfer for 2D model is only in one direction as shown in Fig. 7b (Front and Edge) which represents the cross-sectional view of the model (e.g. the cross-section through the single layer).

Due to the limitation of the 2D model to transport heat only vertically through Aluminum to OHP, an additional layer is introduced to account for heat flow in multiple directions. Fig. 7c represents the 2D 2 Layer model figure where two layers are separated by a depth and heat is conducted from multiple directions. The two layers will also have interfacial resistance present between them. The interfacial thermal resistance for this model is applied to vertical thermal transport which cross the interface between aluminum and OHP channel.

2.2 Governing Equations

The finite-difference numerical model was developed using Fourier's law of heat conduction. An implicit calculation method helps to determine the temperature at each node for the case of both rectangular and cylindrical model geometry. The assumptions made for the numerical model while maintaining the fundamental governing equations include:

a. The oscillating heat pipe material is linearly conductive and treated isotropic. This results in a linear transfer of heat via conduction. This approximation is made as a result of high thermal conductivity of OHP which transfers heat linearly and heat spreads around quickly.

b. An interfacial resistance is present between Al and OHP materials. Due to the addition of interfacial resistance between two materials, the results obtained are in close approximation to experimental work.

c. The PCMs have a sharp boundary between solid-liquid interphase represented by each node. The density of solid and liquid PCM is assumed to be the same.

The number of nodes used along vertical and horizontal directions depends on the height and width of the model used. Both 2D and 2D 2 layer models are based on fundamental governing equations of energy balanced equations.

$$\dot{E}_{in} + \dot{E}_{gen} = \dot{E}_{storage} \quad (1)$$

$\dot{E}_{in}$ is the energy in or heat in via conduction at the boundary of the system. For finite difference method, energy in is conducted via Fourier's law of heat conduction. The term $\dot{E}_{gen}$ is the energy generated by the system, which is assumed to be zero as there is no energy generation in our model. $\dot{E}_{storage}$ is the total increase in sensible and latent heat in the volume of the system.

Fig. 8a represents an internal node for the 2D model of unit depth. $\Delta x$ is the distance between two nodes in x-direction and $\Delta y$ is the distance between two nodes in y-direction. The general equation to determine the temperature of node $i, j$ given by Fourier's heat conduction equation is:

$$k(\Delta y. \Delta z)\frac{T_{i,j-1}^{p+1} - T_{i,j}^{p+1}}{\Delta x} + k(\Delta y. \Delta z)\frac{T_{i,j+1}^{p+1} - T_{i,j}^{p+1}}{\Delta x} + k(\Delta x. \Delta z)\frac{T_{i-1,j}^{p+1} - T_{i,j}^{p+1}}{\Delta y}$$

$$+ k(\Delta x. \Delta z)\frac{T_{i+1,j}^{p+1} - T_{i,j}^{p+1}}{\Delta y} = \rho C_p(\Delta y. \Delta z. \Delta x)\frac{T_{i,j}^{p+1} - T_{i,j}^{p}}{\Delta t} \quad (2)$$

In the above equation, $k$ represents thermal conductivity of material for given node, $\rho$ is density of material and $C_p$ is heat capacity of material. $T_{i,j}^{p}$ is the temperature at node $i, j$ to calculate at time $p$. The Fourier Number is defined as:

$$F_0 = \frac{\alpha t}{x^2} \quad (3)$$

Where, $\alpha$ is thermal diffusivity given by $\alpha = \frac{k}{\rho C_p}$, $t$ is time and $x$ is distance between two nodes along horizontal direction. Solving Eq (2) using the formula of Fourier number and thermal

14

diffusivity value and recombining the terms gives the temperature of node $i, j$ at time $p$.
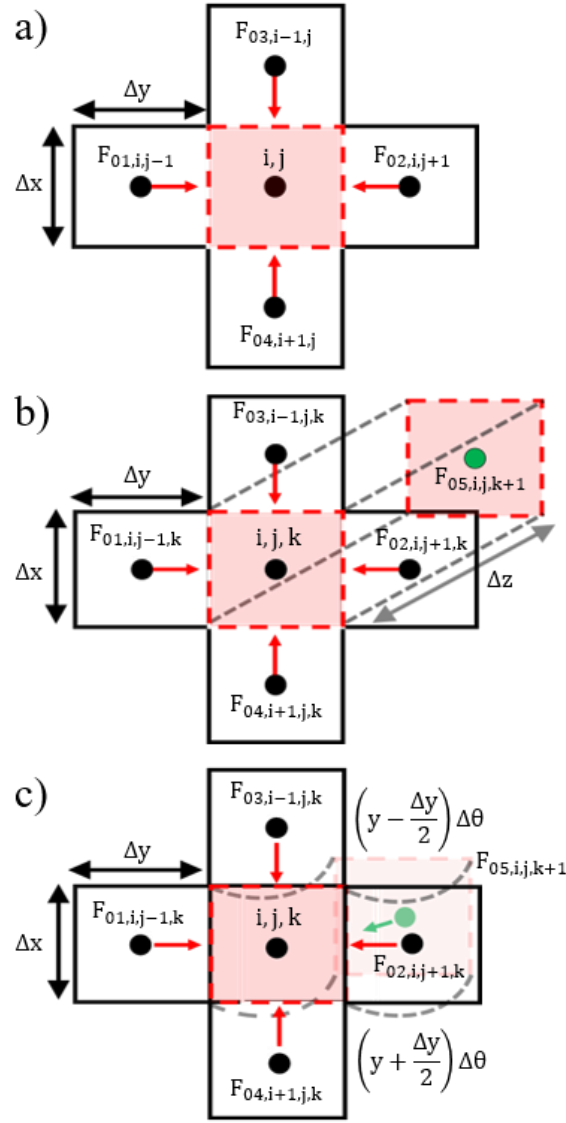


Figure 8: Fourier number representation for a single node a) 2D model b) 2D 2 Layer rectangular model c) 2D 2Layer cylindrical model

$$T_{i,j}^p = (1 + F_{01} + F_{02} + F_{03} + F_{04})T_{i,j}^{p+1} - \left(F_{01}T_{i,j-1}^{p+1} + F_{02}T_{i,j+1}^{p+1} + F_{03}T_{i-1,j}^{p+1} + F_{04}T_{i+1,j}^{p+1}\right) \quad (4)$$

Where, $F_{01}, F_{02}, F_{03}, F_{04}$ are Fourier numbers in all four directions. The 2D model helps to describe model geometry, however, the final temperature obtained for the 2D model greatly varies with the

addition of PCM. This is due to the limitation of the 2D model as interfacial thermal resistance is applied only along the vertical direction providing insufficient heat to the PCM. To address this issue, higher dimensional analysis was performed where additional interfacial resistance can be observed in two directions as shown in Fig. 8b and Fig. 8c for a rectangular and cylindrical model. This results in more heat flow to the OHP for better melting of PCMs.

The 2D 2 layer model has additional depth along the z-direction. The additional layer presented is required to increase the effective heating into PCM system for more melting. The two-layer model is close representative for actual model geometry of OHP. The total depth between two layers is $\Delta z$. However, depending on the depth ratio of each layer, $z_1$ represent total depth of $1^{st}$ layer and $z_2$ represents total depth of $2^{nd}$ layer. The total depth of two-layer model is given by:

$$\Delta z = z_1 + z_2 = l.\Delta z + (1-l).\Delta z \quad (5)$$

Where, $l$ is the depth ratio of two layers. The energy balance equation for two-layer model is similar to Eq. 1 and Fourier's heat conduction equation is similar to Eq. 2 with additional depth along $z$-direction.

$$k(\Delta y. z_1)\frac{T_{i,j-1,k}^{p+1} - T_{i,j,k}^{p+1}}{\Delta x} + k(\Delta y. z_1)\frac{T_{i,j+1,k}^{p+1} - T_{i,j,k}^{p+1}}{\Delta x} + k(\Delta x. z_1)\frac{T_{i-1,j,k}^{p+1} - T_{i,j,k}^{p+1}}{\Delta y}$$

$$+ k(\Delta x. z_1)\frac{T_{i+1,j,k}^{p+1} - T_{i,j,k}^{p+1}}{\Delta y} + k(\Delta y. \Delta x)\frac{T_{i,j,k+1}^{p+1} - T_{i,j,k}^{p+1}}{\Delta z}$$

$$= \rho C_p (\Delta y. z_1. \Delta x)\frac{T_{i,j,k}^{p+1} - T_{i,j,k}^{p}}{\Delta t} \quad (6)$$

Where, $\Delta x, \Delta y,$ and $\Delta z$ is the distance between two nodes for horizontal, vertical and depth of two layers. $T_{i,j,k}^{p}$ represents the temperature to be determined for node $i, j, k$ of $1^{st}$ layer. Solving Eq. 6 provides:

$$T_{i,j,k}^p = \left(1 + F_{01} + F_{02} + F_{03} + F_{04} + \frac{F_{05}}{l}\right) T_{i,j,k}^{p+1}$$

$$- \left(F_{01} T_{i,j-1,k}^{p+1} + F_{02} T_{i,j+1,k}^{p+1} + F_{03} T_{i-1,j,k}^{p+1} + F_{04} T_{i+1,j,k}^{p+1} + \frac{F_{05}}{l} . T_{i,j,k+1}^{p+1}\right) \quad (7)$$

Where, $F_{01}, F_{02}, F_{03}, F_{04}$ and $F_{05}$ represents Fourier number. Eq. 7 is similar to Eq. 4 except the addition of $F_{05}$ which represents the depth of 1st layer of 2D_2Layer model.

The cylindrical model provides better approximation as heat is spread out evenly in all direction. For cylindrical model the depth of model is not constant and keeps on increasing with increase in height. The average depth for each node of cylindrical model as shown in Fig. 6c is:

$$\Delta z = y d\theta \quad (8)$$

Where, y is the vertical distance and $\theta$ is angular distance of the model. The Fourier heat conduction for finite difference method yields the temperature of each node $i, j, k$ as:

$$T_{i,j,k}^p = \left(1 + F_{01} + F_{02} + F_{03}.\frac{\left(y - \frac{\Delta y}{2}\right)}{y} + F_{04}.\frac{\left(y + \frac{\Delta y}{2}\right)}{y} + \frac{F_{05}}{l}\right) T_{i,j,k}^{p+1}$$

$$- \left(F_{01} T_{i,j-1,k}^{p+1} + F_{02} T_{i,j+1,k}^{p+1} + F_{03}.\frac{\left(y - \frac{\Delta y}{2}\right)}{y} T_{i-1,j,k}^{p+1} + F_{04}.\frac{\left(y + \frac{\Delta y}{2}\right)}{y} T_{i+1,j,k}^{p+1}\right.$$

$$\left. + \frac{F_{05}}{l} . T_{i,j,k+1}^{p+1}\right) \quad (9)$$

The cylindrical model geometry provides better approximation and more accurate result as heat is spread evenly throughout.

## 3. RESULTS AND DISCUSSION[*]

3.1 Development of Finite Difference Model

3.1.1 Numerical validation with experimental results for transient thermal response

The 2D numerical model geometry is validated using the numerical simulation at constant heat flux boundary condition on heating side and convective boundary condition on cooling side. The interfacial resistance between two materials, i.e. Al and OHP is introduced, which provides better residual fit with experiment data. For the validation of the model with experimental results, the thermal conductivity value used for better residual fit along x-axis is $K_{OHP,x} = 20$ W·m$^{-1}$·K$^{-1}$ and y-axis is $K_{OHP,y} = 32000$ W·m$^{-1}$·K$^{-1}$. The interfacial resistance value obtained is $R_{int} = 2 \times 10^{-7}$ m$^2$·K·W$^{-1}$. Similarly, the same model geometry was applied to 2D 2 layer model with the length ratio of OHP and Aluminum 0.7:0.3. The heat flux value used for the model is 38600 W·m$^{-2}$ and the convective cooling coefficient value required was 3500 W·m$^2$·K$^{-1}$.
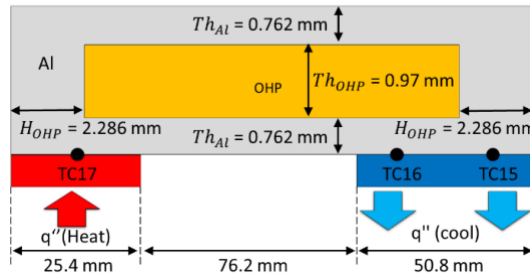


Figure 9: OHP model for validation of 2D and 2D 2 layer model. Reprinted from 2021, IEEE [37]

Three thermocouples were placed for the numerical model. The position of thermocouples are placed in the same position identical to experimental measurement. TC17 is placed at heating

---

[*] Reprinted with permission from "Reduced Order Numerical Model and Design of Hybrid Oscillating Heat Pipe – Phase Change Material Panels" by A. Shrestha, P. Shamberger, B. Alexander, D. Pounds, 2021, 20th IEEE Intersociety Conference on Thermal and Thermomechanical Phenomena in Electronic Systems (iTHERM), 1 June 2021 by IEEE

section and TC15 and TC16 is placed in cooling section to determine the temperature over a period of time. The geometry dimension used for the model is shown in Fig. 9 along with the position of the heating section and cooling section. The OHP is enclosed in Aluminum.

Fig. 10a and 10b represents the temperature and thermocouple position graph at different power levels from 0 W to 50 W. The model temperature and experimental temperature results for 2D and 2D 2 layer rectangular models are close to each other. This is due to the introduction of interfacial resistance between two materials.
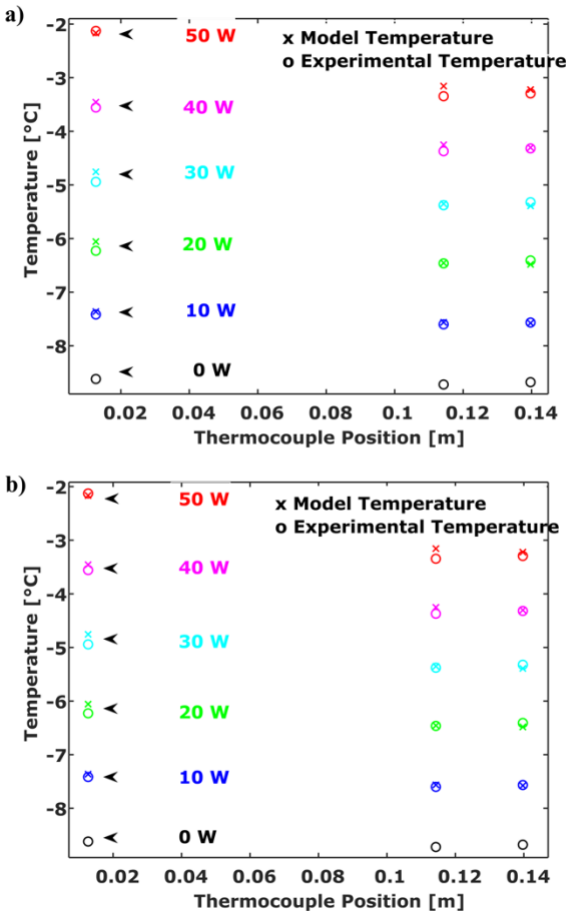


Figure 10: Temperature vs thermocouple position for both numerical and experimental result for a) 2D and b) 2D 2 Layer model. TC15 and TC16 are placed on cold section and TC17 placed on hot section. Reprinted from 2021, IEEE [37].

The two parameters; thermal resistance and interfacial resistance were also highly correlated to each other. The numerical and experimental results average residual obtained for all three thermocouples was 0.2061. After the validation of the numerical model, the transient thermal response of OHP model was evaluated and compared with experimental work prior to adding PCM on the model. This test was performed to evaluate the transient thermal response behavior of the material prior to adding phase change materials into the system.
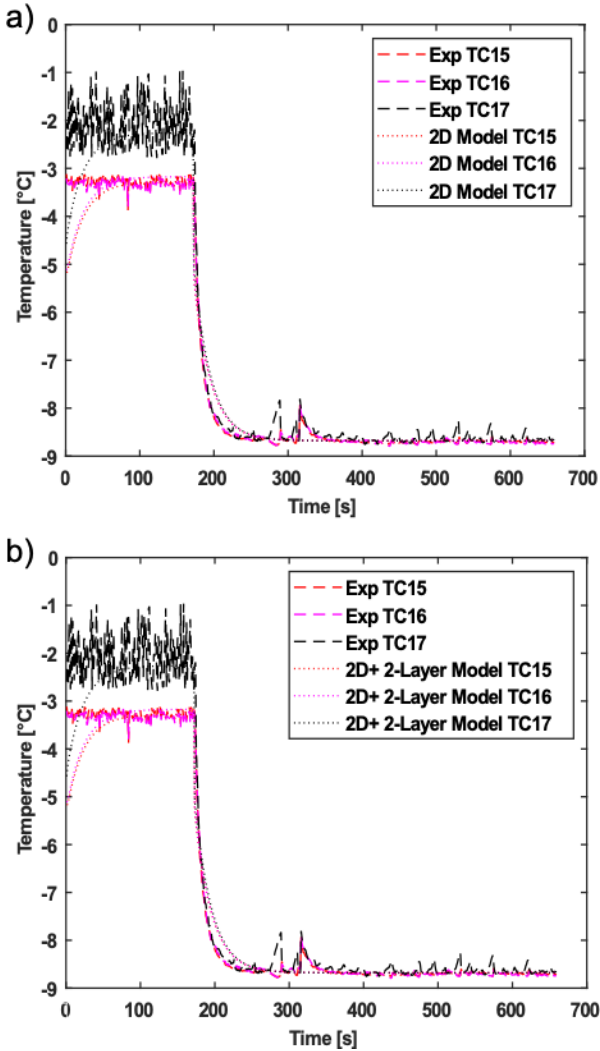


Figure 11: Transient temperature vs time plot for numerical and experimental results for a) 2D model and b) 2D 2 layer model. Reprinted from 2021, IEEE [37].

In order to determine the transient thermal behavior, 50 W power was introduced at the beginning and then turned off at 200 sec to 0 W where the graph obtained for numerical value is in close approximation with experimental work. In Fig. 11a and 11b, we observe small peak areas in the experimental result. The small peak area is associated with incomplete shutdown of power after discharging.

## 3.1.2   Integration of PCM into OHP model*

The new model geometry was defined (Fig. 1c) to analyze melting behavior of PCM into the OHP system at different time steps to determine the dependence of PCM melting with respect to time steps used. The PCM used for the test is octadecane with properties listed in Table 1. The hybrid OHP-PCM model test was performed for model height 0.25 m, width 0.0033 m and depth of 0.001 m. The number of nodes along the height of the panel used is greater than number of nodes along width of the panel. For the test at different timesteps, constant heat flux boundary condition on hot side with adiabatic boundary condition at all other side was used to observe heat loss through heat absorption of PCM. The timesteps used for the tests were 0.02 second, 0.002 second and 0.0002 second for a total time of 10 seconds.

The results of melt fraction is shown in Fig. 12a and 12b. Fig. 12a shows the result for 0.2 millisecond timestep. For both Fig. 12a and 12b, PCMs region is highlighted where melting of PCM occurs, with yellow region as complete melting. Similarly, Fig. 12b shows the melt fraction of PCM at different timesteps from 20 milliseconds to 0.2 milliseconds and also performed for different number of nodes. However, there is no dependence on number of nodes used for melt fraction region hence, lower number of nodes can be used to determine melt fraction to save computational time. For timestep at 20 millisecond, the melt fraction throughout the region spreads

at even rate, for 2 millisecond timestep, we observe some melt fraction occurring more with heat spread occurring horizontally along the direction of OHP channel.
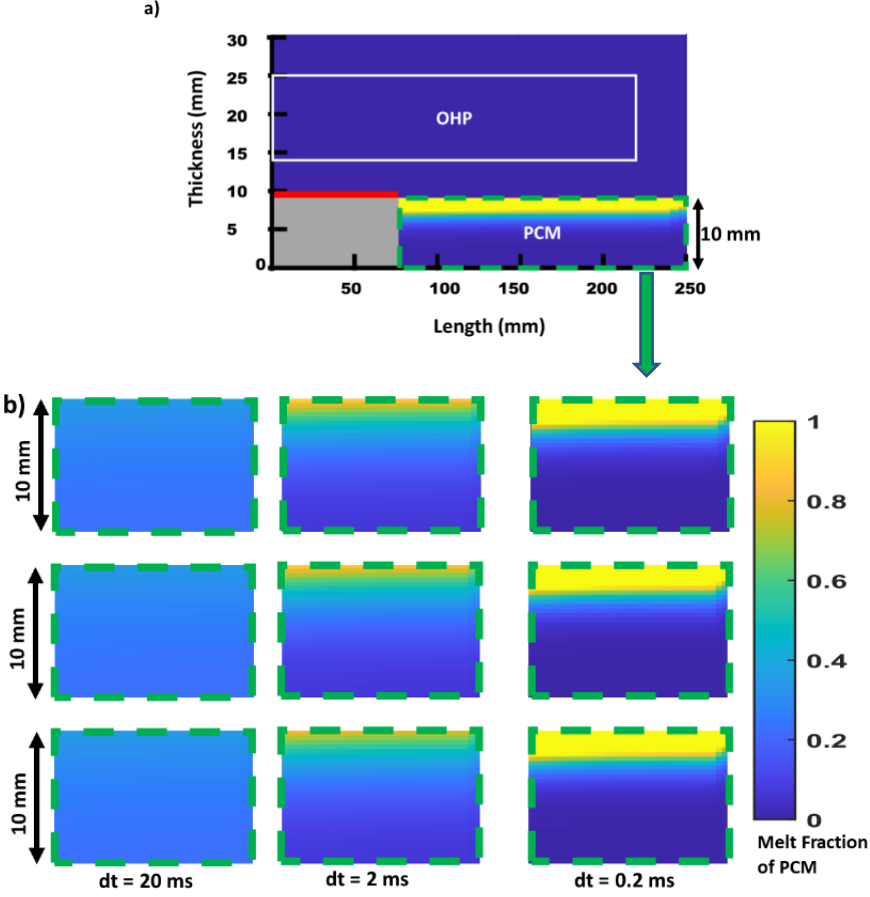


Figure 12: a) Melt fraction of PCM for 2D 2 Layer at timestep 0.2 millisecond for total time 10 second. b) melt fraction at different timestep form 20 millisecond to 0.2 millisecond.  Fig. 10b correspond to PCM melt fraction region shown in Fig.10a. Reprinted from 2021, IEEE [37].

Similarly, at timestep 0.2 millisecond, we observe higher melt fraction at point of contact near heated section with greater heat transfer across the OHP channel and moving towards next spatial region. All three timestep tests were performed for total time of 10 seconds.
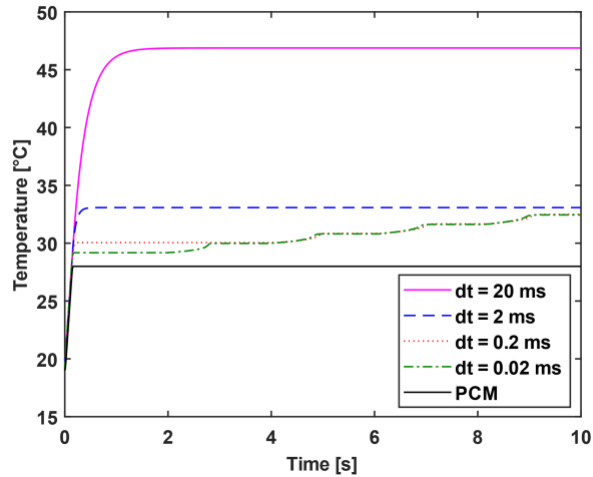
Figure 13: Temperature vs time for different timestep increments from 20 millisecond to 0.02 millisecond. Reprinted from 2021, IEEE [37].

Fig. 13 represents the temperature-time plot at different timesteps ranging from 20 millisecond to 0.02 millisecond. Same boundary conditions were applied for different timestep tests. At a timestep of 20 millisecond, the temperature rises to steady state temperature at 47 ℃ without any transient temperature load. However, for a 2 millisecond timestep, the steady state temperature value reduces to 33 ℃. The difference in temperature between two timesteps for same boundary conditions suggests the importance of timestep during spatial discretization of PCMs for finite volume with sharp boundary between solid and liquid. However, as the timestep is decreased further to 0.2 millisecond, sharp melt-front is observed for PCMs. This results in a discrete step increase in temperature where PCM starts to melt. Similarly, the 0.02 millisecond timestep overlaps 0.2 millisecond timestep and temperature starts to converge. For the study of parameters affecting melting behavior of PCMs, at lower timesteps the temperature starts to converge. Hence, the convergence study resulting in overlapping of temperature-time plot for smaller time step can be used for the numerical simulation to save computational time for long run.

3.2 Results of Numerical Evaluations of Hybrid OHP - PCM Slabs

3.2.1   General thermal response

The thermal response behavior using different PCMs properties at different thickness is similar for

rectangular and cylindrical models. The melting behavior of PCMs for rectangular model is shown

in Fig. 14. The time step used is 0.2 second for a total time of 4000 seconds. PCMs slab of thickness

10 mm and no PCM slab condition results are obtained. The PCM used is Octadecane (C8H18) as

it is non-reactive material with high latent heat fusion. The test was performed for a power of 1

kW or 13123 W/m2 heat flux that reaches the steady-state condition around 250 ℃ after complete

melting of PCM. Constant heat flux boundary condition on hot side and radiation boundary

condition on cooling side is maintained with a thermal emissivity of 0.9. The height and depth of

the slab used is 0.25 m and 1 m. As observed in the Fig. 14, for a model with no PCM slab the

temperature quickly reaches steady state temperature.
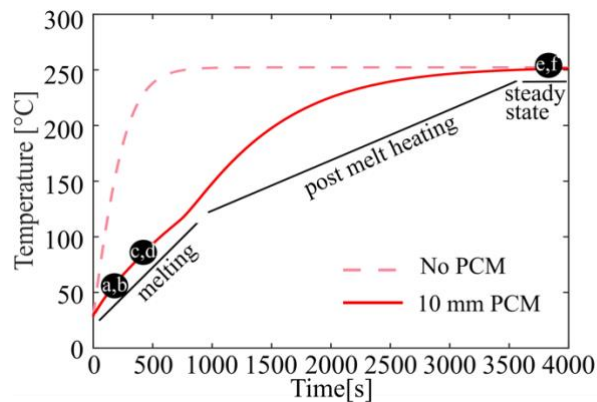


Figure 14: temperature vs time for No PCM slab and 10 mm PCM slab for octadecane.

However, for a 10 mm PCM slab condition, the transient behavior of hybrid OHP/PCM slab is

observed with increase in time before it reaches steady state. This slope represents the melting

behavior of PCMs, where PCMs melts. Around 800 second, there is sudden rise in temperature

after complete melting of PCMs occurs called 'post melt heating'. During post melt heating the

temperature starts to rise uniformly across the slab until it reaches steady-state condition. The time difference to reach 100 ℃ temperature with the addition of 10 mm thick slab of PCM is around 700 seconds. Similarly, the temperature and melt fraction regime at a different time for Fig. 14 is shown in Fig. 15.
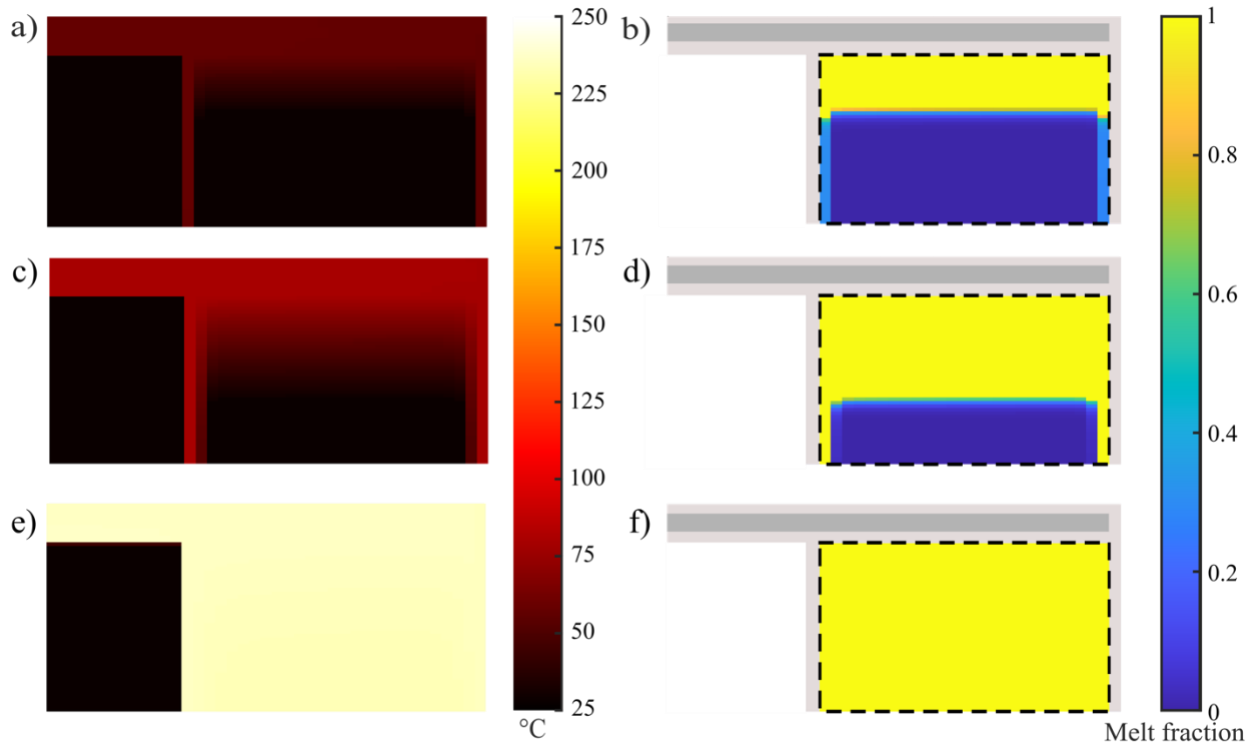


Figure 15: Heat map and melt fraction regime for 200 second, 400 second and 4000 second for 10 mm thick PCM in a rectangular model. a), c), e) represents heat map and b), d), f) represents melt fraction region. a) and b) is for 200 second, c) and d) is for 400 sec and e) and f) is for 4000 second.

Fig. 15 provides temperature map and melt fraction regime for 10 mm thick PCM slab. Fig. 10a, 10b represents temperature map and melt fraction region at time 200 second where melting of PCMs starts to occur. As observed in Fig. 15b, the melting starts to occur at the top represented by yellow color for complete melting. With increase in time, more PCMs starts to melt. At 400 second, almost all PCMs melts shown in Fig 15c and 15d. The temperature keeps on rising as melting is

also occurring. At 800 second, the PCM completely melts and the temperature of OHP/PCM slab reaches uniform around 4000 second as observed in Fig. 15f.

### 3.2.2 Approximate temperature rise at the heated surface during melting

The energy conservation for 2D 2 layer rectangular model and cylindrical model was calculated analytically and compared with model geometry results. The comparison between numerical and analytical calculation results showed close results with $\pm$ 2% of absolute error. The numerical simulation heat rate obtained for the rectangular model is 0.59 W and the analytical solution heat rate is 0.60 W with an absolute error of 1.6 %. Although the same heat rate is expected for both numerical and analytical results, the difference in heat rate observed is due to the computational limit of numerical simulation in terms of numerical resolution and round-off error of each value stored in given nodes. Hence, the conservation of energy is valid within 2 % error. Similarly, the following test is also performed for a cylindrical model using the same model geometry. The numerical simulation heat rate value obtained is 0.73 W and the analytical solution heat rate value obtained is 0.72 W with an error of 1.3 %. For both cases, the error obtained is due to the computational limit or round-off error which is within the range of acceptable error.

The temperature vs time plot was measured for analytical solution with energy balance equation. The similar kind of results are obtained for both rectangular and cylindrical model geometry. The energy balance equation is given as:

$$\dot{Q_{in}} - \dot{Q_{out}} = \dot{Q_{stored}} \quad (10)$$

$$\frac{dQ_{in}}{dt} = \rho C_p V \frac{dT}{dt} + (\rho V L_w)_{PCM} \frac{d\varphi}{dt} \quad (11)$$

Where, $\frac{d\varphi}{dt} = \frac{dx}{dt} \times \frac{1}{L}$

From Fourier's Law of heat conduction,

$$\dot{Q} = kA\frac{dT}{dx} \quad (12)$$

Final Slope of the system from energy balance equation:

$$\frac{dT}{dt} = \left(\frac{\frac{dQ_{in}}{dt} - \left((\rho V L_w)_{PCM} \times \frac{dx}{dt} \times \frac{1}{L}\right)}{(\rho C_p V)_{system}}\right) \quad (13)$$

Eq. 13 is the slope of the system that can be used to determine slope at different powers for analytical calculation.

The slope is used to calculate the temperature-time plot for analytical results and compared against the numerical model. In Fig. 16, the numerical and analytical result slope are shown for rectangular model with PCM octadecane for all three powers.
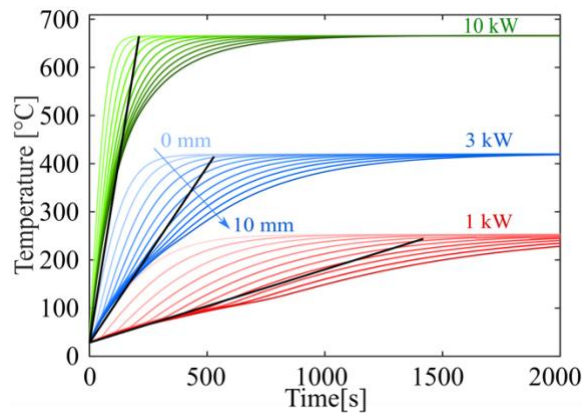


Figure 16: Temperature vs time profile for PCM thickness ranging from 1 mm to 10 mm at three different power of 1 kW, 3 kW and 10 kW for rectangular model with octadecane PCM. The solid black line represents analytical calculation result for all three different power.

The black line represents analytical result and red, blue and green lines represent numerical results at different thickness. The slope line of analytical result shows a good convergence with numerical

27

result. For 1 kW power, the slope starts to deviate more around 300 second because in numerical model we have additional Aluminum strips along the width of PCM storage medium which acts as isothermal with OHP. Hence, with increase in thickness of a material, the slope gets less steep due to presence of Aluminum material that encloses PCM.

## 3.3  Discussion of Hybrid OHP/PCM Slabs Design Features

### 3.3.1  PCM: Octadecane for both rectangular and cylindrical model

The property of phase change material to absorb heat until it reaches the melting point. This helps to reduce the temperature during high heat load which is also called as latent heat. The latent heat property of phase change materials has a high energy storage density. Fig. 15 represents the temperature vs time profile (Fig. 17a,b) and performance vs cost (Fig. 17c,d) of 2D 2 layer rectangular model (Fig. 17a) and cylindrical model (Fig. 17b). The time to reach steady-state condition in both models increases with an increase in PCM thickness. For 1 kW power as observed in Fig. 17a and 17b of both rectangular and cylindrical models, the time to reach steady-state condition is longer compared to 3 kW and 10 kW power. For the purpose of studying transient nature at different power, the transient time period was observed at a temperature limit of 100 ℃ at different power conditions.

Fig. 17c and 17d of both rectangular and cylindrical model geometry shows performance vs cost, where performance is time and cost is mass of the system. For power of 10 kW, large amount of transient time cannot be obtained even when higher mass of octadecane is used. The octadecane melts after 10 second even when higher mass is used for 10 kW power. Hence for 10 kW, the model approaches mass limitation at short time period.

Figure 17: a) Temperature vs time at three different power for 0-10 mm thickness of PCM octadecane for rectangular model. b) Temperature vs time at three different power for cylindrical model. c) performance vs cost tradeoffs at 100 C temperature limit with corresponding mass of the model geometry for rectangular model. d) performance vs cost of cylindrical model. Red line represents 1 kW power, blue line represents 3 kW power and green line represents 10 kW power.

However, with increase in mass of the PCM more time can be gained before it reaches the 100 ℃ temperature limit for 1 kW power. For rectangular model additional time around 580 second is gained before the temperature hits 100 ℃. Similarly, for cylindrical model additional time around 620 second is gained before reaching the temperature limit. Hence, there is tradeoffs of using higher power and gaining more time before reaching the temperature limit.

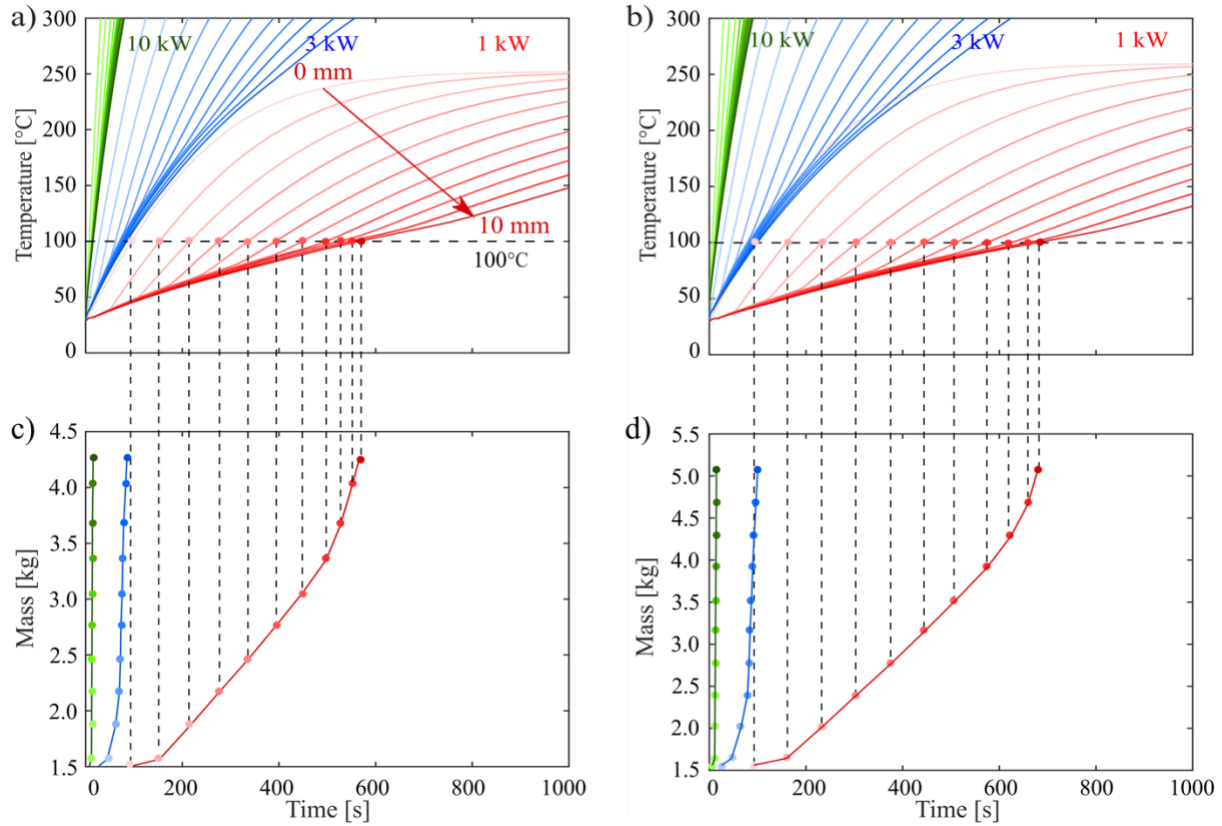### 3.3.2  PCM: Gallium for both rectangular and cylindrical model



Figure 18: a) Temperature vs time at three different power for 0-10 mm thickness of PCM gallium for rectangular model. b) Temperature vs time at three different power for cylindrical model. c) performance vs cost tradeoffs at 100 C temperature limit with corresponding mass of the model geometry for rectangular model. d) performance vs cost of cylindrical model. Red line represents 1 kW power, blue line represents 3 kW power and green line represents 10 kW power.

The comparison of temperature vs time and performance vs cost tradeoffs of PCM gallium was performed for both rectangular and cylindrical model using the properties of gallium. Since, gallium has higher thermal conductivity, lower latent heat of fusion and high density as compared to octadecane, gallium shows greater transient time period compared to octadecane in terms of use of volume but lower performance in terms of use of mass. Fig. 18a represents temperature vs time and Fig. 18c represents cost vs performance for gallium. For the case of gallium, as gallium has

higher density compared to octadecane, it takes long amount of time to melt the PCM and hence has higher energy storage density. In Fig. 18a the temperature vs time plot at three different powers of 1 kW, 3 kW and 10 kW is shown for gallium. The time to reach steady state temperature for gallium is higher than octadecane. To observe the transient nature of the model using gallium, the performance vs cost is observed at temperature limit of 100 ℃ for both rectangular and cylindrical model. At 1 kW power, for 10 mm thick PCM it takes additional time of 1400 second to reach the temperature limit compared to having no PCM in the system. Similar results can be observed for cylindrical model where additional time of around 1600 second is gained before reaching the temperature limit. The performance vs cost tradeoffs for both rectangular and cylindrical model at three different powers can be observed where at high power of 10 kW the time to reach temperature limit is around 100 second for both models and for 3 kW is 400 second for rectangular and 500 second for cylindrical model. Hence, there is tradeoffs of using higher power and lower performance. However, with lower power at 1 kW addition time of around 1400 second for rectangular and 1600 second for cylindrical model can be observed.

### 3.3.3   PCM: Composite(0.9 VF of octadecane and 0.1 VF of Al) for both rectangular and cylindrical model

The role of phase change materials in performance vs cost tradeoffs of pure material such as gallium with low latent heat compared to octadecane but higher density was observed where it takes longer time to reach the temperature limit for the case of gallium. Similarly, the model was run for the case of composite phase change materials using the properties of octadecane and Al using rule of mixture formula where the volume fraction of octadecane used was 0.9 and volume fraction of metal (Al) used was 0.9. The PCM composite has optimized properties of octadecane and gallium where it has higher density than octadecane and high latent heat than gallium. The top
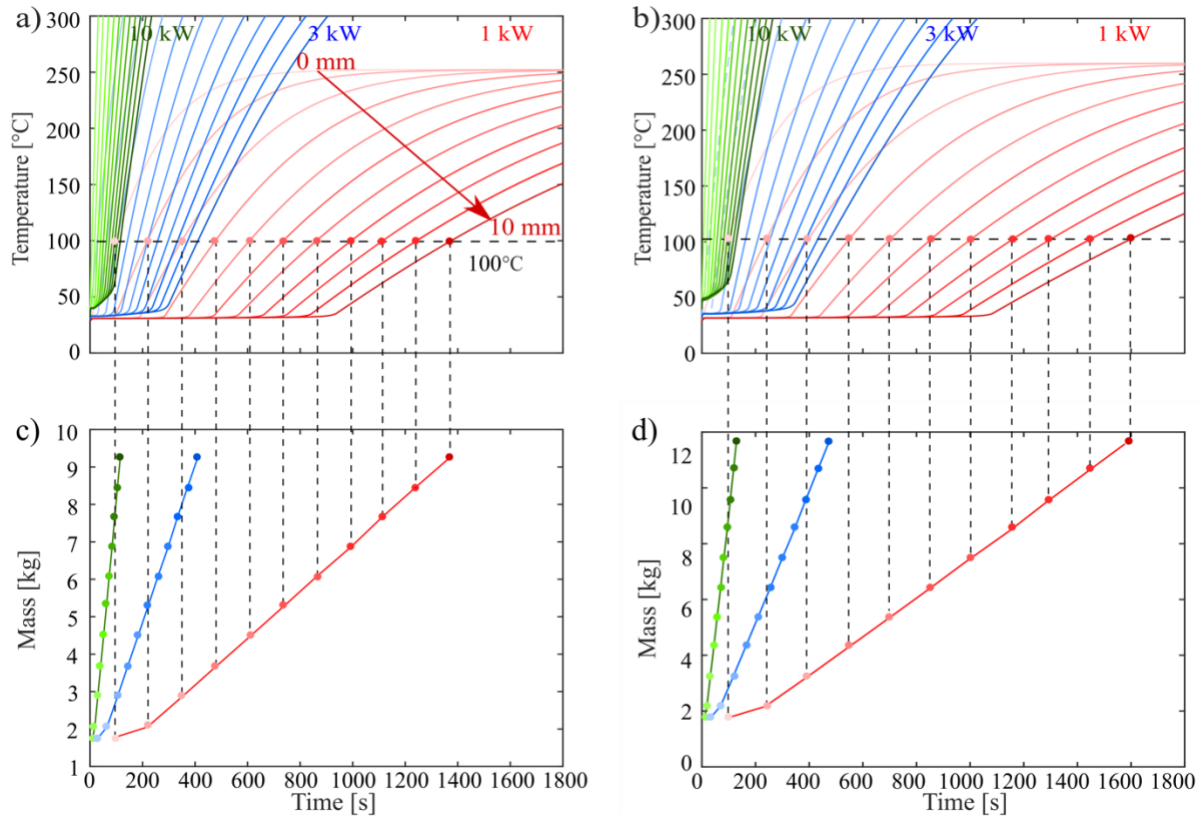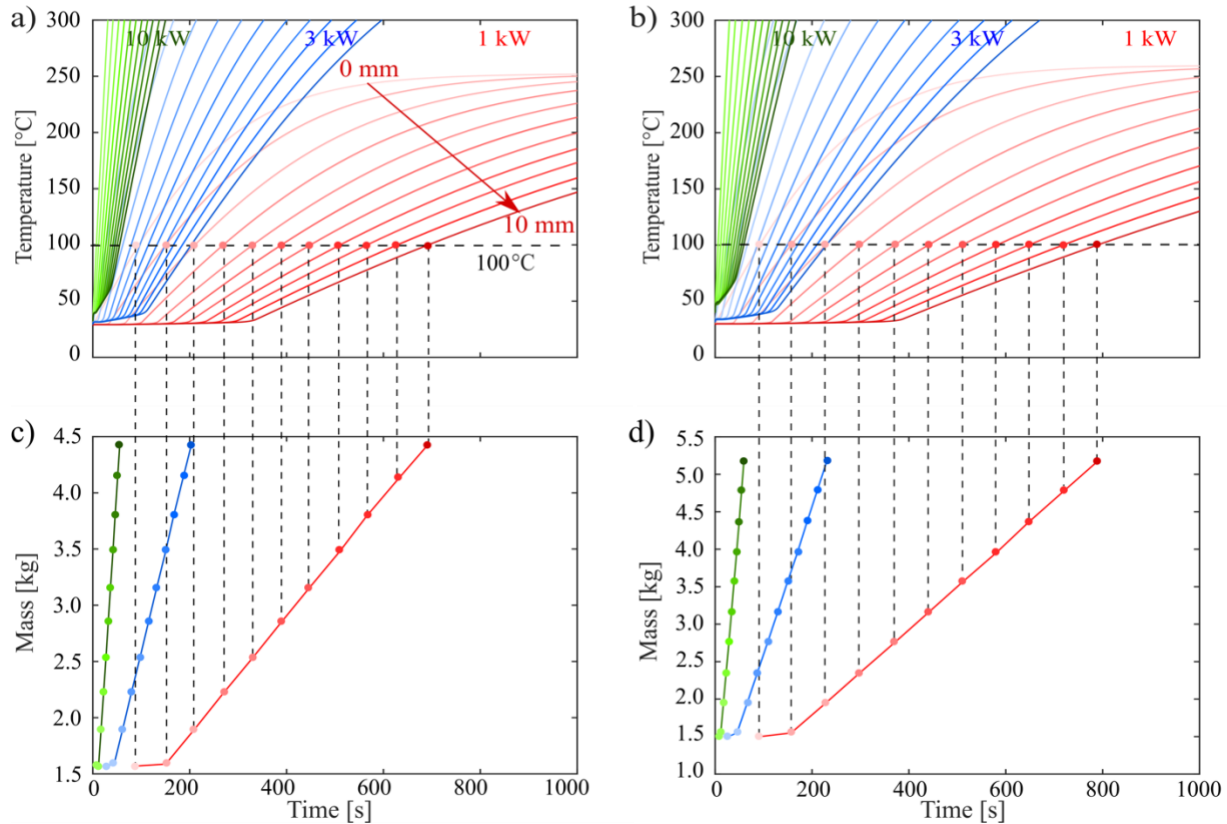
Figure 19: a) Temperature vs time at three different power for 0-10 mm thickness of PCM composite for rectangular model. b) Temperature vs time at three different power for cylindrical model. c) performance vs cost tradeoffs at 100 C temperature limit with corresponding mass of the model geometry for rectangular model. d) performance vs cost of cylindrical model. Red line represents 1 kW power, blue line represents 3 kW power and green line represents 10 kW power.

image in Fig. 19 represents temperature vs time for both rectangular (Fig. 19a) and cylindrical (Fig. 19b) model. The time to reach temperature limit of 100 ℃ at 1 kW power for a 10 mm thick composite is 700 second for rectangular model and around 800 second for cylindrical model. As observed in two previous cases of PCM gallium and octadecane at higher power, the performance is better at higher cost.

### 3.3.4 Comparison of performance vs cost for different PCM at different power
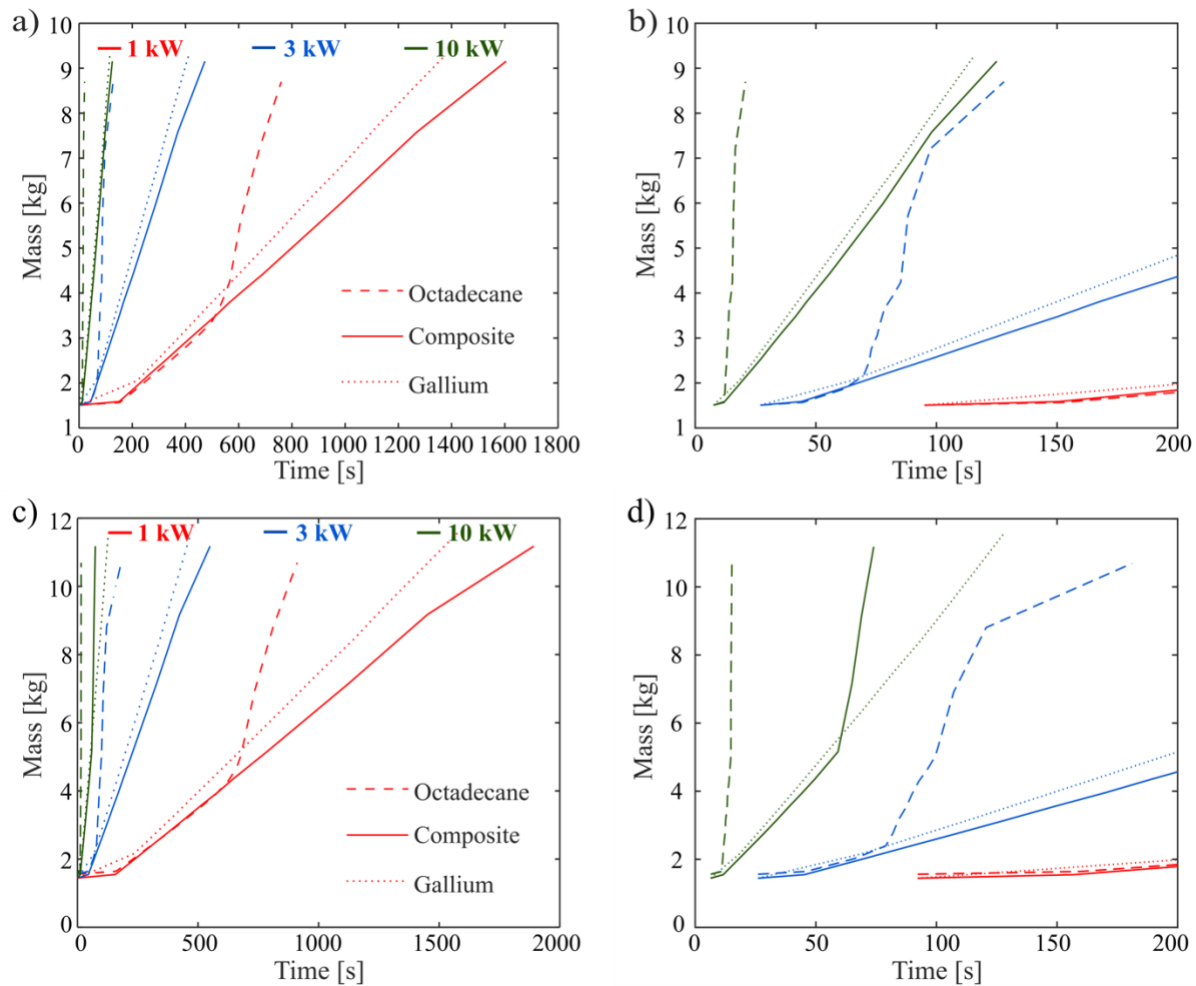


Figure 20: Performance vs cost for different PCM at 100 ℃ . Solid line is composite, dashed line is octadecane and dotted line is gallium. Red line is for 1 kW power, Blue line is for 3 kW power and green line is for 10 kW power. a) rectangular model b) cylindrical model

The performance vs cost of all three PCMs for both rectangular model (Fig. 20 a) and cylindrical model (Fig. 20 c) is compared. The test for all three PCMs was performed at the same conditions. The close view results for up to 200 second is also provided for both rectangular ( Fig. 18b) and cylindrical model (Fig. 20d). As observed in Fig. 20a, for the mass limited case composite outperforms both octadecane and gallium at all three powers. In terms of cost, at lower mass of up

to around 4 kg octadecane outperforms both composite and gallium. However, for higher mass composite outperforms both octadecane and gallium. For rectangular model, at 1 $kW$, octadecane reaches its mass limit around 4 kg and at time around 560 s. The mass additional than 4 kg will not provide higher time to reach 100 C. For the case of composite, even at higher mass we observe that the time also increases linearly. Similarly for the case of gallium the higher mass also results in longer time period. However, in terms of comparing the cost between gallium and composite, composite outperforms gallium as less mass provides higher time period to reach temperature limit. The similar results are obtained for cylindrical model (Fig. 20c), where composite outperforms both octadecane and gallium at higher mass. This is because composite have optimized property between gallium and octadecane. The density of composite is higher than octadecane but less than gallium and latent heat storage is higher than gallium but less than octadecane.

### 3.3.5   Effect on performance vs cost with increase in height of radiator panel

The next design challenge was to observe the performance vs cost with increase in height of the panel by keeping the constant heat flux and radiation boundary conditions. The test was performed at different powers of 1 kW, 3 kW and 10 kW for pcm octadecane, gallium and composite as shown in Fig. 21. The red line represents original height and black line represents 20% increase in height for cylindrical model geometry. The performance was observed for 100 C temperature limit. In Fig. 21a, at 1 kW power for case of octadecane, the mass of original height and 20% increase in intersect around 450 second. At 5 kg mass for both cases, there is additional time increase of 100 sec for 20 % increase in height. Similarly, for the case of gallium and composite with increase in length of radiator panel, the increase in length of radiator panel intersects original height after certain time. The similar trend can be observed for higher powers. At 3 kW, for the case of

octadecane with increase in height, the original height intersects at shorter time period. At Fig. 21 b) for the model to reach 100 C, with increase in height of the panel by 20% it takes additional time of 100 second to reach 100 C temperature limit for octadecane. Similarly for the case of composite the mass intersect around 250 second and for gallium the intersection point is not observed for given mass of up to around 10 kg. The similar kind of results can be observed for 10 kW power, where additional increase in height leads to higher performance for the case of octadecane and composite and intersection point is still not observed for the case of gallium due to limited tests performed.
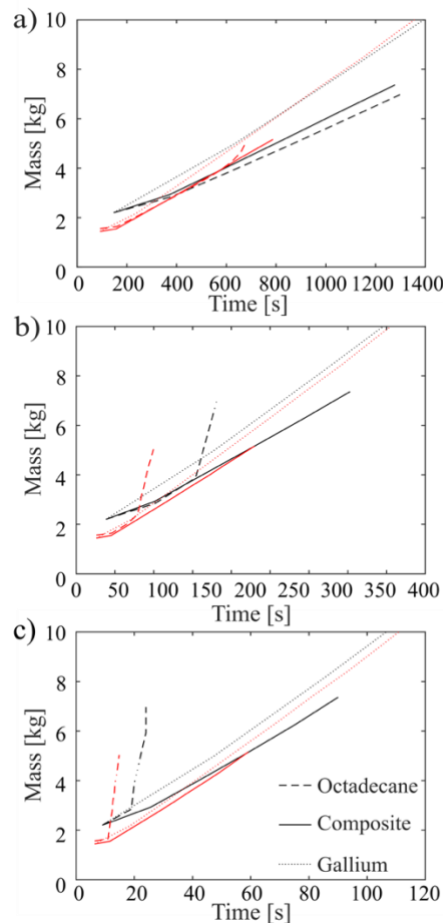


Figure 21:Performance vs cost  for original height (represented in red color) of 0.28 m and 20% increase in height (represented in black color) of 0.34 m at different powers for three PCMs. a) 1 kW, b) 3kW and c) 10 kW

## 4. CONCLUSION

The numerical solution method for hybrid OHP-PCM to measure the thermal performance of the system during transient thermal loading conditions is developed for three different PCMs; octadecane, gallium, and composite (0.9 VF paraffin and 0.1 VF Al). The effect of use of different number of nodes and timestep was studied to observe the PCM melting rate. The number of nodes used for finite volume method up to the thickness of 10 mm introduced for PCM does not affect the PCM melting rate for model geometry and use of small timesteps i.e. 0.02 second provide better melting behavior of PCMs. The general thermal response of OHP-PCM model was also observed for transient loads at different power and thickness of PCMs. For the case of paraffin, additional time of 500 second is required to reach the temperature of 100 ℃ by adding 3.5 kg of PCM into the system. The test results for different power input of 1 kW, 3 kW, and 10 kW also affects the rate of heat transport of hybrid panel and thermal buffering. At low power i.e. 1 kW, we observe high thermal buffering and at high power i.e. 3 kW and 10 kW, we observe low thermal buffering because of high heat transport. The performance of hybrid panel was observed at 100 ℃ temperature limit, where octadecane is limited by rate of heat transport due to low thermal conductivity. As a result, the additional mass into the system does not provide additional time gain. However, gallium and composite (0.9 VF paraffin and 0.1 VF Al) is not limited by rate of heat transport but is limited by volume as complete melting occurs due to higher thermal conductivity. Similarly, the three different PCMs used for the test case shows composite hybrid panel with better performance results in terms of use of mass (cost) compared to paraffin and gallium. The test performed for an additional increase in height of radiator panel shows better transient thermal buffering compared to original height of the model. This model can be used as a general utility

tool to observe the design tradeoffs of mass and volume limited case for different thickness of

PCMs for different power input.

REFERENCES

1. Shang, B., et al., *Passive thermal management system for downhole electronics in harsh thermal environments.* Applied Thermal Engineering, 2017. **118**: p. 593-599.

2. Chauhan, A., V.V. Tyagi, and S. Anand, *Futuristic approach for thermal management in solar PV/thermal systems with possible applications.* Energy Conversion and Management, 2018. **163**: p. 314-354.

3. Rawal, S.P., D.M. Barnett, and D.E. Martin, *Thermal management for multifunctional structures.* IEEE Transactions on Advanced Packaging, 1999. **22**(3): p. 379-383.

4. Ando, M., et al., *On-orbit demonstration of oscillating heat pipe with check valves for space application.* Applied Thermal Engineering, 2018. **130**: p. 552-560.

5. Chaudhry, H.N., B.R. Hughes, and S.A. Ghani, *A review of heat pipe systems for heat recovery and renewable energy applications.* Renewable and Sustainable Energy Reviews, 2012. **16**(4): p. 2249-2259.

6. Miyazaki, Y., F. Polasek, and H. Akachi, *Oscillating heat pipes*. 2000, SAE Technical Paper.

7. Akachi, H., *Structure of a heat pipe*. 1990, Google Patents.

8. Yin, D., et al., *Operation limitation of an oscillating heat pipe.* International Journal of Heat and Mass Transfer, 2016. **94**: p. 366-372.

9. Robak, C.W., T.L. Bergman, and A. Faghri, *Enhancement of latent heat energy storage using embedded heat pipes.* International Journal of Heat and Mass Transfer, 2011. **54**(15-16): p. 3476-3484.

10. Liu, Z., Z. Wang, and C. Ma, *An experimental study on heat transfer characteristics of heat pipe heat exchanger with latent heat storage. Part I: Charging only and discharging only modes.* Energy Conversion and Management, 2006. **47**(7-8): p. 944-966.

11. Singh, R., et al., *Heat pipe based cold energy storage systems for datacenter energy conservation.* Energy, 2011. **36**(5): p. 2802-2811.

12. Shukla, K.N. *Heat Pipe for Aerospace Applicationì An Overview*. 2015.

13. Siricharoenpanich, A., et al., *Thermal management system of CPU cooling with a novel short heat pipe cooling system.* Case Studies in Thermal Engineering, 2019. **15**: p. 100545.

14. Suman, B. and P. Kumar, *An analytical model for fluid flow and heat transfer in a micro-heat pipe of polygonal shape.* International Journal of Heat and Mass Transfer, 2005. **48**(21): p. 4498-4509.

15. Moon, S.H., et al., *Experimental study on the thermal performance of micro-heat pipe with cross-section of polygon.* Microelectronics Reliability, 2004. **44**(2): p. 315-321.

16. Ma, H.B. and G.P. Peterson, *Experimental Investigation of the Maximum Heat Transport in Triangular Grooves.* Journal of Heat Transfer, 1996. **118**(3): p. 740-746.

17.     Chernysheva, M.A., S.I. Yushakova, and Y.F. Maydanik, *Copper–water loop heat pipes for energy-efficient cooling systems of supercomputers.* Energy, 2014. **69**: p. 534-542.

18.     Desai, K., et al., *Investigation on the effect of thermal properties by changing geometry of a heat pipe using simulation.* Materials Today: Proceedings, 2021. **46**: p. 8473-8479.

19.     Wang, G., et al., *Effect of geometries on the heat transfer characteristics of flat-plate micro heat pipes.* Applied Thermal Engineering, 2020. **180**: p. 115796.

20.     Gilmore, D.G. and M. Donabedian, *Spacecraft thermal control handbook: cryogenics.* Vol. 2. 2002: AIAA.

21.     Smoot, C.D. and H.B. Ma, *Experimental Investigation of a Three-Layer Oscillating Heat Pipe.* Journal of Heat Transfer, 2014. **136**(5).

22.     Gi, K., F. Sato, and S. Maezawa. *Flow visualization experiment on oscillating heat pipe.* in *Proc. 11th International Heat Pipe Conference.* 1999.

23.     Groll, M. and S. Khandekar. *Pulsating heat pipes: progress and prospects.* in *Proc. Int. Conf. on Energy and the Environment.* 2003.

24.     Tong, B., T. Wong, and K. Ooi, *Closed-loop pulsating heat pipe.* Applied thermal engineering, 2001. **21**(18): p. 1845-1862.

25.     Xian, H., et al., *Heat transfer characteristics of oscillating heat pipe with water and ethanol as working fluids.* Journal of heat transfer, 2010. **132**(12).

26.     Zhu, Y., et al., *The study on the difference of the start-up and heat-transfer performance of the pulsating heat pipe with water− acetone mixtures.* International Journal of Heat and Mass Transfer, 2014. **77**: p. 834-842.

27.     Ji, Y., et al., *Particle size effect on heat transfer performance in an oscillating heat pipe.* Experimental Thermal and Fluid Science, 2011. **35**(4): p. 724-727.

28.     Xu, J., Y. Li, and T. Wong, *High speed flow visualization of a closed loop pulsating heat pipe.* International Journal of Heat and Mass Transfer, 2005. **48**(16): p. 3338-3351.

29.     Ma, H.B., et al., *Heat Transport Capability in an Oscillating Heat Pipe.* Journal of Heat Transfer, 2008. **130**(8).

30.     Khandekar, S. and M. Groll, *An insight into thermo-hydrodynamic coupling in closed loop pulsating heat pipes.* International Journal of Thermal Sciences, 2004. **43**(1): p. 13-20.

31.     Qu, W. and H.B. Ma, *Theoretical analysis of startup of a pulsating heat pipe.* International Journal of Heat and Mass Transfer, 2007. **50**(11): p. 2309-2316.

32.     Sakulchangsatjatai, P., et al., *Operation modeling of closed-end and closed-loop oscillating heat pipes at normal operating condition.* Applied Thermal Engineering, 2004. **24**(7): p. 995-1008.

33.     Shafii, M.B., A. Faghri, and Y. Zhang, *Thermal modeling of unlooped and looped pulsating heat pipes.* J. Heat Transfer, 2001. **123**(6): p. 1159-1172.

34.     Cheng, P. and H. Ma, *A Mathematical Model of an Oscillating Heat Pipe.* Heat Transfer Engineering, 2011. **32**(11-12): p. 1037-1046.

35.     Qu, J., H.-y. Wu, and P. Cheng, *Thermal performance of an oscillating heat pipe with Al2O3–water nanofluids.* International Communications in Heat and Mass Transfer, 2010. **37**(2): p. 111-115.

36.     Khandekar, S., N. Dollinger, and M. Groll, *Understanding operational regimes of closed loop pulsating heat pipes: an experimental study.* Applied Thermal Engineering, 2003. **23**(6): p. 707-719.

37.     Shrestha, A., et al. *Reduced Order Numerical Model and Design of Hybrid Oscillating Heat Pipe - Phase Change Material Panels*. in *2021 20th IEEE Intersociety Conference on Thermal and Thermomechanical Phenomena in Electronic Systems (iTherm)*. 2021.

38.     Sharma, A., et al., *Review on thermal energy storage with phase change materials and applications.* Renewable and Sustainable energy reviews, 2009. **13**(2): p. 318-345.

39.     Du, K., et al., *A review of the applications of phase change materials in cooling, heating and power generation in different temperature ranges.* Applied Energy, 2018. **220**: p. 242-273.

40.     Jankowski, N.R. and F.P. McCluskey, *A review of phase change materials for vehicle component thermal buffering.* Applied energy, 2014. **113**: p. 1525-1561.

41.     Alshaer, W.G., et al., *Thermal management of electronic devices using carbon foam and PCM/nano-composite.* International Journal of Thermal Sciences, 2015. **89**: p. 79-86.

42.     Stropnik, R. and U. Stritih, *Increasing the efficiency of PV panel with the use of PCM.* Renewable Energy, 2016. **97**: p. 671-679.

43.     Verma, A., S. Shashidhara, and D. Rakshit, *A comparative study on battery thermal management using phase change material (PCM).* Thermal Science and Engineering Progress, 2019. **11**: p. 74-83.

44.     Wu, W.-f., et al., *Study on the effect of shape-stabilized phase change materials on spacecraft thermal control in extreme thermal environment.* Energy Conversion and Management, 2013. **69**: p. 174-180.

45.     Mulligan, J., D. Colvin, and Y. Bryant, *Microencapsulated phase-change material suspensions for heat transfer in spacecraft thermal systems.* Journal of spacecraft and rockets, 1996. **33**(2): p. 278-284.

46.     Gonzalez-Nino, D., et al., *Experimental evaluation of metallic phase change materials for thermal transient mitigation.* International Journal of Heat and Mass Transfer, 2018. **116**: p. 512-519.

47.     Shamberger, P.J., *Cooling capacity figure of merit for phase change materials.* Journal of Heat Transfer, 2016. **138**(2).

48. Gonzalez-Nino, D., et al. *Numerical evaluation of multiple phase change materials for pulsed electronics applications*. in *Heat Transfer Summer Conference*. 2016. American Society of Mechanical Engineers.

49. Shamberger, P.J. and T.S. Fisher, *Cooling power and characteristic times of composite heatsinks and insulants.* International Journal of Heat and Mass Transfer, 2018. **117**: p. 1205-1215.

50. Deckard, M.E., J. Felts, and P.J. Shamberger. *Cooling power and thermal buffering in composite heatsinks*. in *2018 17th IEEE Intersociety Conference on Thermal and Thermomechanical Phenomena in Electronic Systems (ITherm)*. 2018. IEEE.

51. Hoe, A., et al. *A numerical analysis of conductive heat transfer in cylindrical thermal energy storage composites*. in *2019 18th IEEE Intersociety Conference on Thermal and Thermomechanical Phenomena in Electronic Systems (ITherm)*. 2019. IEEE.

52. Weng, Y.-C., et al., *Heat pipe with PCM for electronic cooling.* Applied Energy, 2011. **88**(5): p. 1825-1833.

53. Kim, T.Y., et al., *Numerical study of the spacecraft thermal control hardware combining solid–liquid phase change material and a heat pipe.* Aerospace Science and Technology, 2013. **27**(1): p. 10-16.

54. Zhuang, B., et al., *Experimental investigation on a novel composite heat pipe with phase change materials coated on the adiabatic section.* International Communications in Heat and Mass Transfer, 2019. **100**: p. 42-50.

55. Wang, Q., et al., *Thermal performance of phase change material/oscillating heat pipe-based battery thermal management system.* International Journal of Thermal Sciences, 2016. **102**: p. 9-16.

56. Rao, Z., Y. Huo, and X. Liu, *Experimental study of an OHP-cooled thermal management system for electric vehicle power battery.* Experimental Thermal and Fluid Science, 2014. **57**: p. 20-26.

57. Zhang, Y. and A. Faghri, *Advances and unsolved issues in pulsating heat pipes.* Heat transfer engineering, 2008. **29**(1): p. 20-44.

58. Iwata, N., H. Ogawa, and Y. Miyazaki. *Experimental study of temperature controllable oscillating heat pipe in space thermal environment*. in *40th International Conference on Environmental Systems*. 2010.

59. Okamoto, A., M. Ando, and H. Sugita, *Initial Evaluation of On-Orbit Experiment of Flat-Plate Heat Pipe.* Heat Pipe Science and Technology, An International Journal, 2014. **5**(1-4).

60. Shatikian, V., G. Ziskind, and R. Letan, *Numerical investigation of a PCM-based heat sink with internal fins.* International journal of heat and mass transfer, 2005. **48**(17): p. 3689-3706.

61. Hale, D., *H00WER, M. and 0'Neill, Phase Change Materials Handbook, Lockheed Missi les and Space Company, HuntsviTTe, TATabama*. 1971, Report No. HREC-5183-2.

62. Duggin, M., *The thermal conductivity of liquid gallium.* Physics Letters A, 1969. **29**(8): p. 470-471.

63.     Davis, J.R., *Aluminum and aluminum alloys*. 1993: ASM international.

64.     Shamberger, P., et al., *Dynamics of melting in a slab under harmonic heating and convective cooling boundary conditions.* Journal of Applied Physics, 2020. **128**(10): p. 105102.